SCIENTIFIC REPORTS

OPEN

Ab Initio determination of Cu 3*d* orbital energies in layered copper oxides

Liviu Hozoi[1], Liudmila Siurakshina[1,2], Peter Fulde[3] & Jeroen van den Brink[1]

[1]Institute for Theoretical Solid State Physics, IFW Dresden, Helmholtzstr. 20, 01069 Dresden, Germany, [2]Laboratory of Information Technologies, Joint Institute for Nuclear Research, 141980 Dubna, Russia, [3]Max-Planck-Institut für Physik komplexer Systeme, Nöthnitzer Str. 38, 01187 Dresden, Germany.

SUBJECT AREAS:
CONDENSED MATTER PHYSICS
SPECTROSCOPY
SUPERCONDUCTING MATERIALS
THEORETICAL CHEMISTRY

Received
9 May 2011

Accepted
26 July 2011

Published
16 August 2011

Correspondence and requests for materials should be addressed to L.H. (l.hozoi@ifw-dresden.de)

It has long been argued that the minimal model to describe the low-energy physics of the high T_c superconducting cuprates must include copper states of other symmetries besides the canonical 3$d_{x^2-y^2}$ one, in particular the 3d_{z^2} orbital. Experimental and theoretical estimates of the energy splitting of these states vary widely. With a novel ab initio quantum chemical computational scheme we determine these energies for a range of copper-oxides and -oxychlorides, determine trends with the apical Cu–ligand distances and find excellent agreement with recent Resonant Inelastic X-ray Scattering measurements, available for La_2CuO_4, $Sr_2CuO_2Cl_2$, and $CaCuO_2$.

It is generally accepted that the low-energy physics of the layered Cu oxide compounds in their normal state is reasonably well described by models which incorporate the "in-plane" Cu 3$d_{x^2-y^2}$ and O 2p_x/2p_y orbitals. However, the energy window over which such models provide a qualitatively correct picture is a matter of active research. One additional ingredient which is often invoked is the Cu 3d_{z^2} orbital, perpendicular onto the CuO_2 layers, and the apical O 2p_z functions having σ-type overlap with the Cu 3d_{z^2}. Recent multi-orbital calculations using dynamical mean-field theory[1] show indeed that some of the features of the optical, x-ray absorption, and photoemission spectra can be better reproduced when the Cu 3d_{z^2} orbitals are explicitly included in the many-body treatment. At finite doping, the inclusion of the Cu 3d_{z^2} functions makes a difference even for the low-energy states close to the Fermi level[1].

The off-diagonal coupling between states of x^2-y^2 and z^2 symmetry was actually found to substantially affect the dispersion of the low-energy bands and the shape of the Fermi surface in earlier semiphenomenological models[2,3], density-functional calculations[4], and quantum chemical studies[5]. Moreover, Ohta *et al.*[6] and recently Sakakibara *et al.*[7] suggested that a direct relation exists between the magnitude of T_c and the size of the $d_{x^2-y^2}-d_{z^2}$ splitting. The splittings within the Cu 3*d* shell are also relevant to excitonic models for pairing and high-T_c superconductivity[8,9]. Even if the importance of the Cu 3d_{z^2} state is stressed in this considerable body of work, the actual experimental and theoretical estimates of the energy of this state vary widely.

Sharp features at about 0.4 eV in early optical measurements on La_2CuO_4 and $Sr_2CuO_2Cl_2$ were initially assigned to crystal-field Cu $d_{x^2-y^2}$ to d_{z^2} charge excitations[10]. A different interpretation in terms of magnetic excitations was proposed by Lorenzana and Sawatzky[11] and latter on confirmed by analysis of the resonant inelastic x-ray scattering (RIXS) spectra at the Cu *K* and L_3-edge[12,13]. The RIXS experiments also show that in La_2CuO_4 and $Sr_2CuO_2Cl_2$ the Cu $d_{x^2-y^2}$ to d_{z^2} transitions occur at 1.5–2.0 eV[14], which is substantially larger than the outcome of earlier wavefunction-based quantum chemical calculations, 1.0–1.2 eV[15], or density-functional estimates, 0.9 eV[7].

With the aim to settle this point we employ a recently developed *ab initio* quantum chemical computational scheme to extract the splittings within the Cu 3*d* shell in several layered copper oxides. Excellent agreement is found for La_2CuO_4, $Sr_2CuO_2Cl_2$, and $CaCuO_2$ with recent RIXS measurements[14]. Further, the $d_{x^2-y^2}$ to d_{z^2} excitation energies computed here for La_2CuO_4, $YBa_2Cu_3O_6$, and $HgBa_2CuO_4$ are relevant to models which attempt to establish a direct relation between the relative energy of the out-of-plane d_{z^2} level and the critical temperature T_c[7]. In particular, the large difference between the critical superconducting temperatures of doped La_2CuO_4 and $HgBa_2CuO_4$ was directly attributed to a large difference between the $d_{x^2-y^2}$ to d_{z^2} excitation energies[7].

Results

To study bound, excitoniclike states such as the *d*-*d* charge excitations in copper oxides, we rely on real-space *ab initio* methods. In the spirit of modern multi-scale electronic-structure approaches, we describe a given region around a central Cu site by advanced quantum chemical many-body techniques while the remaining part of the solid is modeled at the Hartree-Fock level. The complete-active-space self-consistent-field (CASSCF) method was used to generate multireference wavefunctions for further configuration-interaction (CI) calculations[16]. In the CASSCF scheme, a full CI is carried out within a limited set of "active" orbitals, i.e., all possible occupations are allowed for those active orbitals. The active orbital set includes in our study all $3d$ functions at the central Cu site and the $3d_{x^2-y^2}$ functions of the Cu nearest neighbor (NN) ions. Strong correlations among the $3d$ electrons are thus accurately described. The final CI calculations incorporate all single and double excitations from the Cu $3s$,$3p$,$3d$ and O $2p$ orbitals on a given CuO_4 plaquette and from the $3d_{x^2-y^2}$ orbitals of the Cu NN's. Such a CI treatment is referred to as SDCI. The CASSCF and SDCI investigations were performed with the MOLPRO quantum chemical software[17].

Both SDCI and RIXS results for the Cu d-level splittings are listed in Table 1. The relative energies of the peaks observed between 1 and 3 eV in the Cu L_3-edge RIXS spectra[14] are the sum of a crystal-field contribution, i.e., an on-site crystal-field splitting E_{cf}, and a magnetic term ΔE_{mgn}. The quantum chemical calculations have been performed to extract E_{cf} for a ferromagnetic (FM) arrangement of the Cu d spins. A SDCI treatment for an antiferromagnetic (AF) alignment of the Cu spins in the embedded cluster of five Cu sites is computationally not feasible (see Methods for details). ΔE_{mgn} accounts for AF order in the ground-state configuration of the Heisenberg antiferromagnet and is determined as follows. First the value for the NN exchange coupling constant J is computed by considering an embedded cluster consisting of two CuO_4 plaquettes. For $CaCuO_2$, for example, we find $J = 0.13$ eV, in good agreement with the theoretical results reported in Ref. [18] and with values from experimental data[11, 13, 14]. With this value of J in hand we return to the cluster with five Cu sites and flip the spin of the central Cu ion. This corresponds to an energy increase $\Delta E = zJ/2 = 2J$, where $z = 4$ is the number of NN's and we neglect the quantum fluctuations. For the crystal-field excited states, the superexchange with the NN Cu $d_{x^2-y^2}$ spins is much weaker for a hole excited into the d_{z^2} orbital and zero by symmetry for a hole into a t_{2g} orbital. This contribution due to intersite $d_{z^2} - d_{x^2-y^2}$ superexchange, $\Delta E' = 2J'$, is not included either in the quantum chemical calculations but in a first approximation we can neglect the weak intersite AF interaction J' involving a d_{z^2} hole. From overlap considerations, J' is only a small fraction of the ground-state superexchange J. For a meaningful comparison between the SDCI and RIXS data, we subtracted in Table 1 from the relative RIXS energies reported in Ref. [14] the term $\Delta E_{mgn} = \Delta E - \Delta E' \approx 2J$ representing the magnetic stabilization of the ground-state configuration with respect to the crystal-field excited states. Since $J \approx 0.13$ eV, $\Delta E_{mgn} \approx 0.26$.

The agreement between our SDCI excitation energies and the results from RIXS is remarkable. As shown in Table 1, the differences between the SDCI and RIXS energies are not larger than 0.15 eV. The only exception is the splitting between the x^2-y^2 and xz/yz levels in $CaCuO_2$, where the SDCI value is 0.3 eV larger than in the RIXS measurements. That an accurate description of neighbors beyond the first ligand coordination shell is crucial is clear from the comparison between our and earlier quantum chemical data. In the calculations described in Ref. [15], only one CuO_6 octahedron or one CuO_5 pyramid was treated at the all-electron level. Farther neighbors were described by either atomic model potentials or point charges. Deviations of 0.4 and 0.6 eV (up to 50%) for the z^2 levels in La_2CuO_4 and $Sr_2CuO_2Cl_2$[15], for example, are mainly due to such approximations in the modeling of the nearby surroundings. The d-level splittings depend after all on the charge distribution at the NN ligand sites. The latter is obviously sensitive to the manner in which other species in the immediate neighborhood are modeled. The quality of the results reported here is directly related to the size of the clusters, i.e., five CuO_4 plaquettes, all apical ligands plus the NN closed-shell metal ions of the central polyhedron.

Superconductivity has not been observed in $Sr_2CuO_2Cl_2$ and $CaCuO_2$. The d-level splittings for three representative cuprate superconductors, i.e., La_2CuO_4, $HgBa_2CuO_4$, and $YBa_2Cu_3O_6$, are listed in Table 2. The maximum T_c's achieved by doping in these three materials are 35, 95, and 50 K, respectively. For the $YBa_2Cu_3O_6$ compound, we here refer to the maximum T_c which can be achieved by Ca doping[19]. The large difference between the critical temperatures in La_2CuO_4 and $HgBa_2CuO_4$ was assigned in Ref. 7 to a large difference between the relative energies of the z^2 states in the two materials. The density-functional results for the splittings between the x^2-y^2 and z^2 levels in La_2CuO_4 and $HgBa_2CuO_4$ are 0.91 and 2.19 eV, respectively[7]. RIXS data are not available for $HgBa_2CuO_4$ and independent estimates for the energy separation between the x^2-y^2 and z^2 states are therefore desirable. While we find a rather similar value for $HgBa_2CuO_4$, of 2.09 eV, the quantum chemical and RIXS results[14] for La_2CuO_4 are substantially larger, about 1.4 eV. This makes the difference between the d-level splittings in the above mentioned compounds less spectacular, i.e., $E_{z^2}^{\mathrm{HBCO}} - E_{z^2}^{\mathrm{LCO}}$ is reduced from 1.3 eV in Ref. [7] to 0.7 eV in the present study, which suggests that the model constructed and the conclusions drawn in Ref. [7] at least require extra analysis.

The distance between the Cu and apical ligand sites increases from 2.40 Å in La_2CuO_4[20] to 2.78 Å in $HgBa_2CuO_4$[21]. The effect of this growth of the apical Cu–O bond length on the relative energy of the z^2 hole state can be understood by using simple electrostatic arguments: when the negative apical ions are closer to the Cu site, less energy is needed to promote the Cu $3d$ hole into the z^2 orbital pointing toward those apical ligands. For $HgBa_2CuO_4$, the lowest crystal-field excitation is therefore to the xy level and requires about 1.3 eV, see Table 2, while the z^2 and xz/yz levels are nearly degenerate and more than 0.5 eV higher in energy. On the other hand, in La_2CuO_4 the lowest crystal-field excitation is to the z^2 orbital, see Table 1. Our results also reproduce the near degeneracy between the z^2 and xy levels in La_2CuO_4, as found in the RIXS experiments. In $CaCuO_2$, there are no apical ligands. The splitting between the x^2-y^2 and z^2 levels is therefore the largest for $CaCuO_2$, about 2.4 eV, see Table 1.

Table 1 | CASSCF+SDCI versus RIXS results for the Cu d-level splittings in La_2CuO_4, $Sr_2CuO_2Cl_2$, and $CaCuO_2$ (eV). The ground-state Cu $t_{2g}^6 d_{z^2}^2 d_{x^2-y^2}^1$ configuration is taken as reference. A $2J$ term was here substracted from each of the RIXS values reported in Ref. [14], see text.

Hole orbital	La_2CuO_4 SDCI/RIXS	$Sr_2CuO_2Cl_2$ SDCI/RIXS	$CaCuO_2$ SDCI/RIXS
x^2–y^2	0	0	0
z^2	1.37/1.44	1.75/1.71	2.38/2.39
xy	1.43/1.54	1.16/1.24	1.36/1.38
xz,yz	1.78/1.86	1.69/1.58	2.02/1.69

Table 2 | Cu d-level energy splittings for La_2CuO_4, $HgBa_2CuO_4$, and $YBa_2Cu_3O_6$ (eV). CASSCF+SDCI calculations for 5-plaquette FM clusters.

Hole orbital	La_2CuO_4	$HgBa_2CuO_4$	$YBa_2Cu_3O_6$
x^2–y^2	0	0	0
z^2	1.37	2.09	1.47
xy	1.43	1.32	1.22
xz,yz	1.78	1.89	1.57

Discussion

The parameter that plays the major role in determining the size of the d-level splittings in layered cuprates is clearly the apical Cu–ligand distance. There are, however, few other factors which come into play such as the number and nature of the apical ligands, the in-plane Cu–O bond lenghts, buckling of the CuO_2 planes, and the configuration of the farther surroundings. Trends concerning the relative energy of the z^2 hole state in different cuprates are illustrated in Fig. 1, which includes data for systems having one apical O site ($YBa_2Cu_3O_6$), two apical O's (La_2CuO_4, $HgBa_2CuO_4$), two apical Cl ions ($Ca_2CuO_2Cl_2$, $Sr_2CuO_2Cl_2$) or no apical ligand ($CaCuO_2$). The apical Cu–O distances in La_2CuO_4 and $YBa_2Cu_3O_6$, for example, are nearly the same, 2.40 vs. 2.45 Å[19, 20, 22]. In $YBa_2Cu_3O_6$, however, there is a single apical O. For this reason the z hole state is somewhat destabilized in $YBa_2Cu_3O_6$ and lies above the xy hole configuration, see Table 2. Yet since the Cu ion is shifted towards the apical ion, out of the basal O plane, the x^2-y^2 hole state is also destabilized such that the splitting between the x^2-y^2 and z^2 levels is finally close to the value found in La_2CuO_4. Further, the apical Cu–ligand distances are slightly larger in $Sr_2CuO_2Cl_2$ as compared to $HgBa_2CuO_4$, 2.86 vs. 2.78 Å, respectively. The apical ions also have a smaller effective charge in $Sr_2CuO_2Cl_2$, which should lead to a larger relative energy of the z^2 hole state in $Sr_2CuO_2Cl_2$ as compared to $HgBa_2CuO_4$. The fact that the relative energy of the z^2 hole state is actually larger in $HgBa_2CuO_4$, see Fig. 1, must be related to the smaller in-plane Cu–O distances in $HgBa_2CuO_4$, 1.94 in $HgBa_2CuO_4$ vs. 1.99 Å in $Sr_2CuO_2Cl_2$, which stabilizes the ground-state x^2-y^2 hole configuration in the former compound, and to farther structural details. From $Ca_2CuO_2Cl_2$ to $Sr_2CuO_2Cl_2$, the Cu–Cl separation increases from 2.75 to 2.86 Å[23, 24] and the energy of the z^2 level from 1.37 to 1.75 eV.

In contrast to the z^2 orbitals, the relative energies of the xy levels display much smaller variations, in an interval of 1.2–1.5 eV, see Tables 1 and 2. Substantially smaller are also the variations computed for the xz/yz levels, in an energy window between 1.6 and 2.0 eV.

To summarize, we employ state of the art quantum chemical methods to investigate the Cu 3d electronic structure of layered Cu oxides. Multiconfiguration and multireference configuration-interaction calculations are carried out on finite clusters including five CuO_4 plaquettes plus additional apical ligand and closed-shell metal ion NN's. The localized Wannier functions attached to these atomic sites are obtained from prior Hartree-Fock computations for the periodic system. Excellent agreement is found between our theoretical results and recent Cu L_3-edge RIXS data for La_2CuO_4, $Sr_2CuO_2Cl_2$, and $CaCuO_2$. RIXS is a novel experimental tool to investigate both magnetic and charge excitations with high resolution and accuracy. Our computational scheme and present results indicate a promising route for the modeling and reliable interpretation of RIXS spectra in correlated 3d-metal compounds. A next step along this path is the computation of transition probabilities and intensities at the *ab initio* level, which requires the explicit calculation of the intermediate Cu 3p core hole wavefunctions.

Further, the excitation energies computed here for La_2CuO_4, $YBa_2Cu_3O_6$, and $HgBa_2CuO_4$ are relevant to models which attempt to establish a direct relation between the critical temperature T_c and the strength of the $(x^2-y^2)-z^2$ coupling. For La_2CuO_4, in particular, the density-functional estimate used as input parameter in such models[7] is about 0.5 eV smaller than our result. Consequently, the difference we find between the $d_{x^2-y^2}-d_{z^2}$ splittings in La_2CuO_4 and $HgBa_2CuO_4$ is less spectacular as compared to the value reported by Sakakibara *et al.*[7], suggesting a reevaluation of the analysis in Ref. [7].

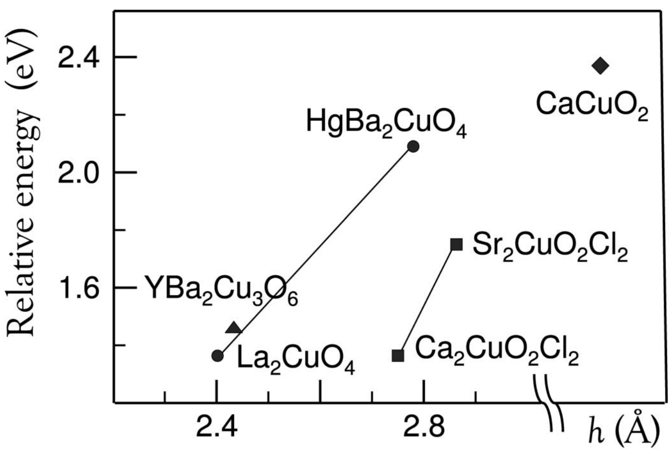

Figure 1 | Relative energy of the Cu z^2 level as function of the distance h between the Cu and apical ligands in different cuprates. There are two apical O sites in La_2CuO_4 and $HgBa_2CuO_4$, two apical Cl sites in $Ca_2CuO_2Cl_2$ and $Sr_2CuO_2Cl_2$, and one apical O ion in $YBa_2Cu_3O_6$. In $CaCuO_2$ the apical ligands are absent.

Methods

The first step in our study is a restricted Hartree-Fock (RHF) calculation for the ground-state configuration of the periodic system. The RHF calculations are performed with the CRYSTAL package[25]. We employed experimental lattice parameters[14, 20–24] and Gaussian-type atomic basis sets, i.e., triple-zeta basis sets from the CRYSTAL library for Cu, O, and Cl plus basis sets of either double-zeta or triple-zeta quality for the other species. Post Hartree-Fock many-body calculations are subsequently carried out on finite clusters, which are sufficient because of the local character of the correlation hole. They consist of five CuO_4 plaquettes, i.e., a "central" CuO_4 unit plus the four NN plaquettes. When present, the apical ligands, oxygen or chlorine, are incorporated as well in the finite cluster $\mathcal{C}$. Additionally, the finite cluster $\mathcal{C}$ includes in each case the NN closed-shell metal ions around the "central" Cu site. In La_2CuO_4, for example, there are ten La^{3+} NN's. In $YBa_2Cu_3O_6$, there are one Cu^{1+} $3d^{10}$, four Y^{3+}, and four Ba^{2+} NN's.

The orbital basis entering the post Hartree-Fock correlation treatment is a set of projected RHF Wannier functions: localized Wannier orbitals (WO's) are first obtained with the Wannier-Boys localization module[26] of the CRYSTAL package and subsequently projected onto the set of Gaussian basis functions associated with the atomic sites of $\mathcal{C}$[27]. Moreover, the RHF data is used to generate an effective embedding potential for the five-plaquette fragment $\mathcal{C}$. This potential is obtained from the Fock operator in the RHF calculation[27] and models the surroundings of the finite cluster, i.e., the remaining of the crystalline lattice.

The central CuO_4 plaquette and the four NN Cu sites form the active region of the cluster, which we denote as $\mathcal{C}_A$. The other ions in $\mathcal{C}$, i.e., each ligand coordination cage around the four Cu NN's and the NN closed-shell metal ions, form a buffer region $\mathcal{C}_B$ whose role is to ensure an accurate description of the tails of the WO's centered in the active part $\mathcal{C}_A$[27]. For our choice of $\mathcal{C}_B$, the norms of the projected WO's centered within the active region $\mathcal{C}_A$ are not lower than 99.5% of the original crystal WO's. While the occupied WO's in the buffer zone are kept frozen, all valence orbitals centered at O and Cu sites in $\mathcal{C}_A$ (and their tails in $\mathcal{C}_B$) are further reoptimized in multiconfiguration CASSCF calculations. In the latter, the ground-state wavefunction and the lowest four crystal-field excited states at the central Cu site are computed simultaneously in a state-averaged multiroot calculation[16]. The d-level splittings at the central Cu site are finally obtained at the CASSCF+SDCI level of theory as the relative energies of the crystal-field excited states. The virtual orbital space in the multireference SDCI calculation cannot be presently restricted just to the $\mathcal{C}_A$ region. It thus includes virtual orbitals in both $\mathcal{C}_A$ and $\mathcal{C}_B$, which leads to very large SDCI expansions, $\sim 10^9$ Slater determinants for a FM configuration. For this reason, we restrict the CASSCF+SDCI calculations to FM allignment of the Cu d spins.

The effective embedding potential is added to the one-electron Hamiltonian with the help of the CRYSTAL-MOLPRO interface program[28]. Although the WO's at the atomic sites of $\mathcal{C}$ are derived for each of the compounds discussed here by periodic RHF calculations for the Cu $3d^9$ electron configuration, the embedding potentials are obtained by replacing the Cu^{2+} $3d^9$ ions by closed-shell Zn^{2+} $3d^{10}$ species. This is a good approximation for the farther 3d-metal sites, as the comparison between our results and RIXS data shows. An extension of our embedding scheme toward the construction of open-shell embeddings is planned for the near future.

1. Weber, C., Haule, K. & Kotliar, G. Apical oxygens and correlation strength in electron- and hole-doped copper oxides. *Phys. Rev. B* **82**, 125107 (2010).
2. Eskes, H. & Sawatzky, G. A. Single-, triple-, or multiple-band Hubbard models. *Phys. Rev. B* **44**, 9656–9666 (1991).
3. Raimondi, R., Jefferson, J. H. & Feiner, L. F. Effective single-band models for the high-Tc cuprates. II. Role of apical oxygen. *Phys. Rev. B* **53**, 8774–8788 (1996).
4. Pavarini, E., Dasgupta, I., Saha-Dasgupta, T., Jepsen, O. & Andersen, O. K. Band-Structure Trend in Hole-Doped Cuprates and Correlation with T_{cmax}. *Phys. Rev. Lett.* **87**, 047003 (2001).

5. Hozoi, L., Laad, M. S. & Fulde, P. Fermiology of cuprates from first principles: from small pockets to the Luttinger Fermi surface. *Phys. Rev. B* **78**, 165107 (2008).
6. Ohta, Y., Tohyama, T. & Maekawa, S. Apex oxygen and critical temperature in copper oxide superconductors: universal correlation with the stability of local singlets. *Phys. Rev. B* **43**, 2968–2982 (1991).
7. Sakakibara, H., Usui, H., Kuroki, K., Arita, R. & Aoki, H. Two-orbital model explains the higher transition temperature of the single-layer Hg-cuprate superconductor compared to that of the La-cuprate superconductor. *Phys. Rev. Lett.* **105**, 057003 (2010).
8. Cox, D. L., Jarrell, M., Jayaprakash, C., Krishna-murthy, H. R. & Deisz, J. Virtual electric quadrupole fluctuations: a mechanism for high T_c. *Phys. Rev. Lett.* **62**, 2188–2191 (1989).
9. Little, W. A. *et al.* A determination of the pairing interaction in the high T_c cuprate superconductor $Tl_2Ba_2CaCu_2O_8$. *Physica C* **460–462**, 40–43 (2007).
10. Perkins, J. D. *et al.* Mid-infrared optical absorption in undoped lamellar copper oxides. *Phys. Rev. Lett.* **71**, 1621–1624 (1993).
11. Lorenzana, J. & Sawatzky, G. A. Phonon assisted multimagnon optical absorption and long lived two-magnon states in undoped lamellar copper oxides. *Phys. Rev. Lett.* **74**, 1867–1870 (1995).
12. Hill, J. P. *et al.* Observation of a 500 meV collective mode in $La_{2-x}Sr_xCuO_4$ and Nd_2CuO_4 using resonant inelastic x-ray scattering. *Phys. Rev. Lett.* **100**, 097001 (2008).
13. Braicovich, L. *et al.* Dispersion of magnetic excitations in the cuprate La_2CuO_4 and $CaCuO_2$ compounds measured using resonant x-ray scattering. *Phys. Rev. Lett.* **102**, 167401 (2009).
14. Moretti Sala, M. *et al.* Energy and symmetry of *dd* excitations in undoped layered cuprates measured by Cu L_3 resonant inelastic x-ray scattering. *New J. Phys.* **13** 043026 (2011).
15. de Graaf, C. & Broer, R. Midinfrared spectrum of undoped cuprates: *d-d* transitions studied by ab initio methods. *Phys. Rev. B* **62**, 702–709 (2000).
16. Helgaker, T., Jørgensen, P. & Olsen, J. *Molecular Electronic-Structure Theory* (Wiley, Chichester, 2000).
17. MOLPRO 2006, Cardiff University, United Kingdom.
18. Muñoz, D., Muñoz, D., de, P. R. Moreira, I. & Illas, F. Effective *t-J* model Hamiltonian parameters of monolayered cuprate supercon-ductors from ab initio electronic structure calculations. *Phys. Rev. B* **65**, 224521 (2002).
19. McCarron, E. M., Crawford, M. K. & Parise, J. B. Observation of superconductivity in $(Y_{1-x}Ca_x)Ba_2Cu_3O_6$. *J. Solid State Chem.* **78**, 192–196 (1989).
20. Longo, J. M. & Raccah, P. M. The structure of La_2CuO_4 and $LaSrVO_4$. *J. Solid State Chem.* **6**, 526–531 (1973).
21. Wagner, J. L. *et al.* Structure and superconductivity of $HgBa_2CuO_{4+\delta}$. *Physica C* **210**, 447–454 (1993).
22. Katano, S. *et al.* Structure of Tetragonal $YBa_2Cu_3O_{5.8}$. *Jpn. J. Appl. Phys.* **26**, 1049–1051 (1987).
23. Argyriou, D. N. *et al.* Structure and superconductivity without apical oxygens in $(Ca,Na)_2CuO_2Cl_2$. *Phys. Rev. B* **51**, 8434–8437 (1995).
24. Miller, L. L. *et al.* Synthesis, structure, and properties of $Sr_2CuO_2Cl_2$. *Phys. Rev. B* **41**, 1921–1925 (1990).
25. CRYSTAL 2000, University of Torino, Italy.
26. Zicovich-Wilson, C. M., Dovesi, R. & Saunders, V. R. A general method to obtain well localized Wannier functions for composite energy bands in linear combination of atomic orbital periodic calculations. *J. Chem. Phys.* **115**, 9708–9719 (2001).
27. See Hozoi, L., Birkenheuer, U., Stoll, H. & Fulde, P. Spin-state transition and spin-polaron physics in cobalt oxide perovskites: ab initio approach based on quantum chemical methods. *New J. Phys.* **11**, 023023 (2009) and references therein.
28. CRYSTAL-MOLPRO interface, Max-Planck-Institut für Physik komplexer Systeme Dresden, Germany.

Acknowledgements

We thank V. Bisogni, L. Braicovich, G. Ghiringhelli, K. Wohlfeld, and V. Yushankhai for fruitful discussions. L. H. acknowledges financial suport from the German Research Foundation (Deutsche Forschungsgemeinschaft, DFG).

Author contributions

L.H., P.F., and J.v.d.B. wrote the main manuscript text, L.H. and L.S. prepared figure 1. All authors reviewed the manuscript.

Additional information

Competing Financial Interests: Authors have no Competing Financial Interests.

How to cite this article: Hozoi, L., Siurakshina, L., Fulde, P. & van den Brink, J. *Ab Initio* determination of Cu 3*d* orbital energies in layered copper oxides. *Sci. Rep.* **1**, 65; DOI:10.1038/srep00065 (2011).